Engineering stability in NADPH oxidases: A common strategy for enzyme production

Marta Ceccon, Elisa Millana Fananas, Marta Massari, Andrea Mattevi & Francesca Magnani

Published online: 10 Jan 2019.

Submit your article to this journal

Article views: 980

View related articles

View Crossmark data

Citing articles: 2 View citing articles

Taylor & Francis
Taylor & Francis Group

Check for updates

ORIGINAL ARTICLE

Engineering stability in NADPH oxidases: A common strategy for enzyme production

Marta Ceccon [ID], Elisa Millana Fananas [ID], Marta Massari [ID], Andrea Mattevi [ID] and Francesca Magnani [ID]

Department of Biology and Biotechnology, University of Pavia, Pavia, Italy

ABSTRACT

NADPH oxidases (NOXs) are membrane enzymes whose sole function is the generation of reactive oxygen species. Humans have seven NOX isoenzymes that feature distinct functions in immune response and cell signaling but share the same catalytic core comprising a FAD-binding dehydrogenase domain and a heme-binding transmembrane domain. We previously described a mutation that stabilizes the dehydrogenase domain of a prokaryotic homolog of human NOX5. The thermostable mutant exhibited a large 19 °C increase in the apparent melting temperature (app T_m) and a much tighter binding of the FAD cofactor, which allowed the crystallization and structure determination of the domain holo-form. Here, we analyze the transferability of this mutation onto prokaryotic and eukaryotic full-length NOX enzymes. We found that the mutation exerts a significative stabilizing effect on the full-length NOX5 from both *Cylindrospermum stagnale* (app T_m increase of 8 °C) and *Homo sapiens* (app ΔT_m of 2 °C). Enhanced thermal stability resulted in more homogeneous preparations of the bacterial NOX5 with less aggregation problems. Moreover, we also found that the mutation increases the overall expression of recombinant human NOX4 and NOX5 in mammalian cells. Such a 2–5-fold increase is mainly due to the lowered cell toxicity, which leads to higher biomasses. Because of the high sequence identity of the catalytic core within this family of enzymes, this strategy can be a general tool to boost the production of all NOXs.

Abbreviations: NOX: NADPH oxidase; csNOX5: NADPH oxidase 5 from Cylindrospermum stagnale NOX5; app T_m: apparent melting temperature; ROS: reactive oxygen species

Introduction

NADPH oxidases (NOX) catalyze the transfer of electrons across biological membranes to produce reactive oxygen species (ROS) on the membrane outer side. The NOX family comprises seven members (NOX1-5, DUOX1-2) that feature the same catalytic cycle but largely differ in their regulatory mechanism and tissue distribution. ROS produced by NOXs have several biological functions, such as the defense against pathogens, cellular signaling, and cell differentiation (Brown & Griendling, 2009; Lambeth, 2004). In healthy cells, ROS mediate a delicate balance between two opposite effects: proliferation and cell death (Block & Gorin, 2012; Irani et al., 1997). Initially, ROS act as mitogenic signaling cues, but then, as oxidative stress increases over time, cells die. Their prolonged and sustained generation is causative of oxidative stress (Kuroda et al., 2010), neurodegenerative diseases (Gao et al., 2012), and senescence (Weyemi et al., 2012).

Moreover, NOX deficiency can cause immunosuppression (NOX2), hypothyroidism (DUOX), and defective otoconogenesis (NOX3) (O'Neill et al., 2015). In plants, genes homologous to NOX5 called Respiratory Burst Oxidase Homologs (RBOH) are involved in stress signaling (Mittler et al., 2011; Zhu, 2016). Comprehensive reviews related to the functions of NOX enzymes in human physiology and pathology can be found (Bedard & Krause, 2007; Lambeth & Neish, 2014).

NOXs are transmembrane proteins. They all share a two-domain catalytic core comprising a domain made of six transmembrane helices with four histidines that coordinate two heme groups, and a C-terminal cytosolic dehydrogenase domain that binds FAD and NADPH. Electrons are sequentially transferred from the substrate NADPH to the cofactor FAD and then to the two heme prosthetic groups. The final acceptor of electrons, bound on the outer side of the membrane, is dioxygen that is reduced to form a superoxide
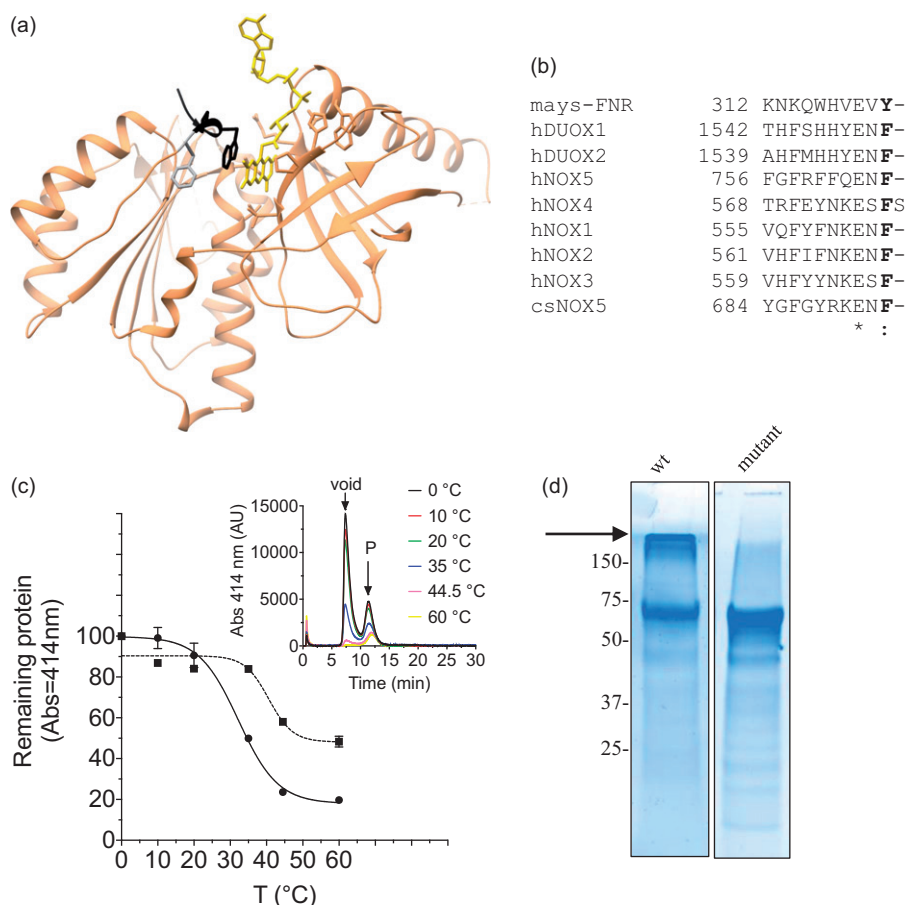
(a)

(b)

```
mays-FNR     312 KNKQWHVEVY-
hDUOX1      1542 THFSHHYENF-
hDUOX2      1539 AHFMHHYENF-
hNOX5        756 FGFRFFQENF-
hNOX4        568 TRFEYNKESFS
hNOX1        555 VQFYFNKENF-
hNOX2        561 VHFIFNKENF-
hNOX3        559 VHFYYNKESF-
csNOX5       684 YGFGYRKENF-
                          * :
```

(c)

(d)

Figure 1 The PWLELAAA insertion stabilizes the full-length csNOX5. (A) csDH three-dimensional structure with bound FAD (carbons in yellow; PDB ID code: 5O0X). The C-terminal PW^{695}LELAAA extension is in black and Phe693 is in gray. **(B)** Sequence alignment of the human NOX family members, *C. stagnale* NOX5, and zea mays Ferredoxin: NADP$^+$ reductase (FNR). The conserved aromatic residue is indicated in bold. Alignment produced with Clustal Omega. **(C)** Melting curves for csNOX5 were obtained by incubating the purified enzymes at the indicated temperatures for 1 h, followed by quenching on ice, centrifugation, and then subjected to size exclusion chromatography. Heme retention was followed by monitoring its absorbance at 414 nm (inset, peak indicated as "P"). The remaining fraction of the heme-containing protein was normalized against the control (0 °C). Data from two experiments performed in duplicate were analyzed by nonlinear regression using Prism software (GraphPad). Values representing the means ± the standard error mean were as follows: wild type (continuous line) = 32.2 ± 1.1 °C, F693^{insPWLELAAA} mutant (dashed line) = 40.6 ± 1.9 °C. For some of the data points, the error bars are the same size or smaller than the symbols. D) Coomassie stained SDS-PAGE of purified full-length csNOX5, wild type (left lane) and F693^{insPWLELAAA} (right lane): the arrow points to aggregated protein. Mass spectrometry confirmed that the protein in the two samples is csNOX5.

anion, the precursor of other highly reactive oxygen species (Ohye & Sugawara, 2010). We recently solved the first three-dimensional crystal structures of the dehydrogenase and transmembrane domains using NOX5 from *Cylindrospermum stagnale* as a reference system (csNOX5), a close homolog of the human NOX5 (Magnani et al., 2017). The atomic models highlighted the key features in the electron transfer pathways and revealed a cluster of conserved residues that are likely to form the oxygen-binding site in proximity of the outer heme. These structural features are fully consistent with the notion that NOXs reduce dioxygen through an outer sphere mechanism that does not require the covalent binding of dioxygen to the iron of the heme (Isogai et al., 1995).

The main obstacle to the structural and biophysical investigation of NOX's catalysis and regulation has been the difficulty in obtaining well-behaved proteins in sufficient amounts. Most efforts have focused on the purification of NOX2 from native source or recombinant expression (de Mendez & Leto, 1995; Lord et al., 2008; Ostuni et al., 2010; Rotrosen et al., 1992, 1993; Segal, 1987). However, so far the yield and stability of these preparations have not been sufficient to proceed with structural studies. The overexpression of NOXs can be highly toxic to cells, particularly for the constitutively active NOX4, with consequent loss of biomass and final protein yield. Moreover, upon extraction from the membranes, these enzymes tend to proteolyze spontaneously and lose their non-

covalently bound cofactors (FAD and hemes). Therefore, a different approach must be devised to produce NOXs in a stable form. The key for the successful crystallization of the csNOX5 dehydrogenase domain was the discovery of a mutation that led to a pronounced increase in protein stability. Specifically, the addition of a short peptide at the C-terminus of the protein (csDH-F693^{extPWLELAAA}) led to a 19 °C increase in the apparent melting temperature (app T_m) associated with a much tighter binding of FAD and allowed the crystallization of the domain in the holo-form (Magnani et al., 2017). As suggested by the three-dimensional structure, the stabilizing effect is caused by the stacking of the newly added Trp695, located in the inserted peptide, against the isoalloxazine ring of the FAD (Figure 1(A)). Trp695 occupies the binding site for NADPH, and this explains the 10-fold reduced catalytic activity of the mutant domain with respect to the wild-type protein. Sequence comparison shows that the C-terminal portion of NOX enzymes is rather well conserved across the NOX family (Figure 1(B)). Therefore, we set out to verify whether this mutation would improve the expression and purification of other NOXs. Our data demonstrate that the mutation can be successfully grafted onto other NOXs with beneficial effects on enzyme production indicating that it might represents a valuable tool for further structural, biochemical, and enzymological studies.

Materials and methods

Expression and purification of full-length csNOX5. The cDNA encoding for the β-isoform of *Cylindrospermum stagnale* NOX5 was purchased from GeneScript and sub-cloned into a modified pET28b carrying an N-terminal FLAG-(His)8-SUMO tag. The plasmid was used to transform *E. coli* BL21 (DE3) RP Plus (Novagen). The transformed cells were grown in 2xTY media at 37 °C with appropriate antibiotics until OD600 reached 1.2. Over-expression of csNOX5 was induced by the addition of 0.4 mM IPTG, and the temperature was shifted to 17 °C for 16 h. Cells were harvested by centrifugation, resuspended in lysis buffer (50 mM Hepes, pH 7.5, 300 mM NaCl, 20% (v/v) glycerol), and supplemented with protease inhibitors (1 μM leupeptine, 1 μM pepstatine, and 1 mM PMSF). All subsequent steps were carried out at 4 °C. After sonication, the lysed cells were centrifuged at 3000 × g for 15 min to get rid of cell debris and the membranes were isolated by centrifugation at 72,000 × g for 45 min. The pellet was resuspended in solubilization buffer to a final protein concentration of 10 mg/mL measured by the Biuret assay (50 mM Hepes pH 7.5, 300 mM NaCl, 20% (v/v) glycerol, 1% (w/v) n-dodecyl-β-D-maltoside). Solubilization proceeded for 2 h. The solubilized sample was centrifuged, and the supernatant was loaded onto an anti-FLAG resin (Anti-DYKDDDDK G1 Affinity Resin, GenScript). The resin was washed with lysis buffer containing 0.03% (w/v) n-dodecyl-β-D-maltoside and eluted with elution buffer (50 mM Hepes pH 7.5, 300 mM NaCl, 5% (v/v) glycerol, 0.03% n-dodecyl-β-D-maltoside, 100 μg/mL FLAG peptide). The insertion PWLELAAA was added after the codon corresponding to F693 (construct F693^{extPWLELAAA}) using the In-fusion (Clontech) method following the manufacturer's instructions. The corresponding mutant protein was purified following the same protocol as for the wild-type csNOX5.

Thermal stability assay for csNOX5. The apparent T_m values for csNOX5 wild-type and F693^{extPWLELAAA} mutant were measured by monitoring the loss of heme (absorbance at 414 nm) with increasing temperature, as described (Magnani et al., 2017). Briefly, the purified wild-type and mutant csNOX5 were divided in aliquots. Each sample was incubated for 1 h at different temperatures. After 30-min centrifugation (16,000 × g, 4 °C), 22 μg of each sample was applied to a Superdex 200 Increase 5/150 GL column (GE Healthcare) equilibrated in buffer (50 mM Hepes pH 7.5, 300 mM NaCl, 5% (w/w) glycerol, 0.03% n-dodecyl-β-D-maltoside (w/v)) maintained at 16 °C. Size-exclusion chromatography was run using a HPLC (Shimadzu) with a flow rate of 0.15 mL/min. The peak amplitude at 414 nm was plotted *vs* T (°C). The data were fitted to the function "sigmoidal dose–response (variable slope)" to calculate the apparent T_m using the Prism software (GraphPad).

Superoxide measurements on membranes containing csNOX5. The activity of wild-type and mutant csNOX5 was evaluated employing csNOX5-containing membrane fractions and cytochrome c (Sigma), which is used as electron acceptor; 90 μg of membranes, containing 1.1 μM csNOX5 (wild-type or mutant), was mixed in a cuvette in buffer (50 mM Hepes pH 7.5, 300 mM NaCl, 20% (w/w) glycerol) containing 2 mM sodium azide, 100 μM cytochrome c and 50 μM FAD. After setting the blank, 200 μM NADPH was added to the solution. Superoxide generation was monitored by following the increase in absorbance at 550 nm due to reduction of cytochrome c by superoxide. To activate the enzyme, 1 mM CaCl$_2$ was added to the sample. Negative controls were performed by adding superoxide dismutase or the inhibitor diphenyleneiodonium (DPI) (Doussiere et al., 1999) in the pre-incubation

Table 1. Kinetic characterization of csNOX5 wild type and mutant.

									Δk_{cat}
50 μM FAD	-		+		+		+		
DPI	-		+		-		-		
SOD	-		-		+		-		
1 mM CaCl2	-	+	-	+	-	+	-	+	
wt	1.08 ± 0.78	0.57 ± 0.1	3.13 ± 0.65	4.7 ± 1.08	1.16 ± 0.66	1.5 ± 0.55	6.8 ± 4	17.4 ± 4.4	10.6 ± 5.9
F693[insPWLELAAA]	0.98 ± 0.16	0.89 ± 0.37	1.2 ± 0.22	0.88 ± 0.14	0.99 ± 0.42	0.76 ± 0.25	1.6 ± 0.46	1.24 ± 0.14	-0.3 ± 0.4

The catalytic activity of csNOX5 was measured by cytochrome c assay reduction as described in Methods. Experiments were carried out in duplicates. Values are representative of two to three independent experiments and plotted as mean ± standard deviation.

buffer, or by omitting FAD in the reaction mixture. Initial rates for cytochrome c reduction were measured by following the ΔAbs at 550 nm 17 sec after NADPH and Ca^{2+} addition. The apparent k_{cat} was calculated considering the extinction coefficient of reduced cytochrome c from bovine heart (28 mM^{-1} cm^{-1}; from Sigma, product number C3131). The concentration of the protein was estimated based on the absorbance of the membranes at 414 nm after subtracting the absorption of control membranes (not expressing csNOX5) using the extinction coefficient 132 mM^{-1} cm^{-1} (Magnani et al., 2017). The apparent k_{cat} values for the mutant and wild-type csNOX5 are listed in Table 1.

Expression of human NOX4 and NOX5 in mammalian HEK293-F cells. The cDNA encoding for the human NOX4 (isoform 1) and NOX5 (isoform β) was synthesized by GeneArt. The plasmids for mammalian cell expression were generated by cloning the cDNA between the BamHI and NotI restriction sites of a modified vector pCMV or pEG-BacMam vector (a kind gift from Eric Gouaux, Oregon Health & Science University, USA) (Goehring et al., 2014). The pCMV vector contains a Kozak sequence, a hexa-histidine tag, a eGFP moiety, a tobacco mosaic virus (TEV) recognition site, and BamHI and NotI restriction sites. The modified pEG-BacMam vector contains a Sal I restriction site, a Kozak sequence, a FLAG tag, a tobacco mosaic virus (TEV) recognition site, followed by BamHI and NotI restriction sites. For NOX4 experiments, cells were co-transfected with a plasmid encoding for p22phox protein cloned in a pcDNA3.1 + (GeneScript). For cloning in the pEG-BacMam vector, the human NOX5 gene was modified by PCR to add at its 5′ a Kozak sequence followed by a FLAG tag and a TEV protease recognition site. Variants of the NOX4 and NOX5 genes were produced by the In-fusion (Clontech) method following the manufacturer's instructions. The HEK293-F cells were grown in suspension using FreeStyle medium (Invitrogen). The day before transfection, cells were seeded at a density of 5×10^5/mL in a six-well plate (2 mL of cells/well). Transient transfection of HEK293-F was performed using polyethylenimine (linear MW

25000, Polyscience Europe GmbH) in a ratio 1:3 (DNA:polyethylenimine, w/w) as described (Tom et al., 2008). The amount of plasmid transfected per mL of culture was 1 μg for NOX5 or 0.5 μg p22phox plus 0.5 μg NOX4. Equivalent amounts of the corresponding empty vector were used as negative control, as indicated in the figure legends. Experiments were performed 48 h after transfection, unless otherwise noted. Expression levels were evaluated by measuring the fluorescence of the GFP moiety genetically fused to the human NOX proteins using a CLARIOstar Plate Reader (BMG LABTECH; excitation 488 nm/emission 512 nm). Cell viability was evaluated by Trypan blue exclusion assay. Cells were mixed to an equal volume of 0.4% Trypan Blue solution (w/v, Sigma) and counted using a hemocytometer (non-viable cells take up the dye and show as blue).

Western blotting. Cells were lysed in 50 mM Hepes pH 7.5, 300 mM NaCl, 20% (v/v) glycerol, 1% (w/v) n-dodecyl-β-D-maltoside, and supplemented with protease inhibitors (Complete-EDTA free, Roche). Lysates were clarified by centrifugation at 16,000 × g for 20 min at 4 °C. Proteins were separated by 12% SDS-PAGE and blotted onto PVDF (Bio-Rad, CA). Membranes were blocked in PBS (phosphate-buffered saline) containing 5% milk and then incubated with an anti-FLAG HRP-conjugated monoclonal antibody (Sigma).

Superoxide measurements on human NOX5-overexpressing whole cells. The cell-permeable fluorophore dihydroethidium was used to measure the cellular production of superoxide. Dihydroethidium is a blue fluorescent dye that is oxidized by superoxide to a red fluorescent product, which intercalates within the DNA. For each data point, 50,000 human NOX5-overexpressing cells were used. 48 h after transfection, cells were washed once with PBS and incubated with 5 μM dihydroethidium for 20 min at 30 °C. Subsequently, 100 nM phorbol 12-myristate 13-acetate was added to the cells followed, after 15 min, by the addition of 1 mM CaCl$_2$ and 1 μM ionomycin to activate the enzyme. Fluorescence signal was recorded using a CLARIOstar Plate Reader (BMG LABTECH) with 524 nm

Table 2. Apparent Tm of NOX constructs.

NOX construct	appT$_m$		
	WT	Trp mutant	ΔappT$_m$ (°C)
csNOX5[a]	32.2 ± 1.1	40.6 ± 1.9	8.3 ± 2.2
hNOX5[b]	40.4 ± 0.9	43 ± 0.7	2.6 ± 1.1
hNOX4[b]	39.2 ± 2.2	37.1 ± 1.7	−2.1 ± 2.8

[a]Purified protein; [b]cell lysates.
Purified csNOX5 proteins (a) and lysates (b) of cells expressing either hNOX5 or hNOX4 as GFP fusions were processed as described in Methods and subjected to size-exclusion chromatography, as described in Figure 1(C) legend and Methods. Data were analyzed using the Prism software (GraphPad). Values represent the means ± the standard error mean of two experiments performed in duplicate.

excitation and 606 nm emission wavelengths every 5 min for 40 min at 30 °C. The value reported corresponds to the 40-min time point.

Horseradish peroxidase coupled amplex red assay to measure hydrogen peroxide production in NOX4-overexpressing cells. Cells overexpressing human NOX4s were counted, sedimented in a centrifuge (1000 × g, 5 min at room temperature), resuspended in PBS, and dispensed in a black 96-well plate (for each data point 50,000 NOX-overexpressing cells in 50 μL were prepared). For each data point, an appropriate volume of a pre-mix was made containing 12.5 μM Amplex Red (Invitrogen) and 2.5 μg horseradish peroxidase. Right before the assay, 50 μL of pre-mix was added to the cells and measurement was started. Fluorescence was measured on a CLARIOstar Plate Reader (BMG LABTECH) with 535 nm excitation and 595 nm emission wavelengths every 5 min for 40 min at 30 °C. The value reported corresponds to the 40-min time point.

Thermal stability assay for human NOX5 and NOX4. The apparent T$_m$ for the human NOX4 and NOX5 was estimated by monitoring the decrease in the GFP fluorescence (emission at 520 nm) with increasing temperature (Hattori et al., 2012). 5 mL cell culture was sedimented at 800 × g for 5 min at room temperature. The pellet was resuspended in lysis buffer (0.5% n-dodecyl-β-D-maltoside (w/v), 500 mM NaCl, 50 mM Hepes pH 7.5, 5% glycerol (w/w), protease inhibitors (Complete-EDTA free, Roche)). Solubilization proceeded for 1 h at 4 °C, and supernatant was collected after centrifugation for 30 min (16.000 × g, 4 °C). The sample was divided in seven aliquots of 100 μL each, and incubated for 1 h at different temperatures. After centrifugation for 40 min (16.000 × g, 4 °C), 50 μL of each sample was applied on a Superdex 200 5/150 GL (GE Healthcare) equilibrated in buffer (50 mM Hepes pH 7.5, 330 mM NaCl, 5% glycerol (w/w), 0.03% n-dodecyl-β-D-maltoside (w/v)) maintained at 16 °C. Size-exclusion chromatography was run on a HPLC (Shimadzu) with a flow rate of 0.15 mL/min, and the maximum peak's height (%) at 520 nm was plotted *vs*

T (°C). Data were fitted to the function "sigmoidal dose–response (variable-slope)" to calculate the apparent T$_m$ using the Prism software (GraphPad).

Results

Grafting the PWLELAAA peptide into the full-length csNOX5

The C-terminal dehydrogenase domain of NOXs can be produced and purified as soluble protein which is endowed with an oxidase activity that results from the NADPH-dependent reduction and oxygen-dependent re-oxidation of the domain-bound FAD (Magnani et al., 2017). We have previously described the dehydrogenase domain of csNOX5 (residues 413–693). In particular, we have uncovered a domain variant that contains an extending PWLELAAA sequence after Phe693, the C-terminal residue of the protein (Figure 1(A,B)). This F693[extPWLELAAA] mutant showed a 5-fold slower rate in NADPH consumption compared to the wild-type domain and strongly enhanced thermal stability (Magnani et al., 2017). Specifically, the mutated domain exhibited a striking 19 °C increase in the melting temperature. Consistently, the F693[extPWLELAAA] mutation was essential to obtain the crystals that were employed for structure determination of the dehydrogenase portion of csNOX5 (Magnani et al., 2017).

To explore the applicability of this stabilizing mutation to other NOXs, we decided to first transfer the F693[extPWLELAAA] extension to the full-length csNOX5. Recombinant proteins were expressed in *E. coli* cells, and their catalytic activities were measured using isolated cell membranes and cytochrome c as electron acceptor. NOX5 is activated by the binding of Ca^{2+} to N-terminal calcium-binding EF domain, and therefore, 1 mM Ca^{2+} was added to the cell membranes to trigger enzyme activation. The F693[extPWLELAAA] csNOX5 had no detectable ROS-producing activity compared to the wild-type protein (Table 1). This is in agreement with the csDH-F693[extPWLELAAA] domain mutant, where the tryptophan within the extension PWLELAAA hinders access of NADPH to its binding pocket, thus inhibiting electron transfer and ROS production (Magnani et al., 2017). Next, the apparent melting temperatures of the enzymes were measured. To this aim, the purified wild-type or mutant csNOX5 were heated at various temperatures, centrifuged to eliminate precipitated protein, and analyzed by analytical size-exclusion chromatography. The loss of heme due to protein unfolding was monitored by following its distinctive absorbance at 414 nm. Protein kept on ice
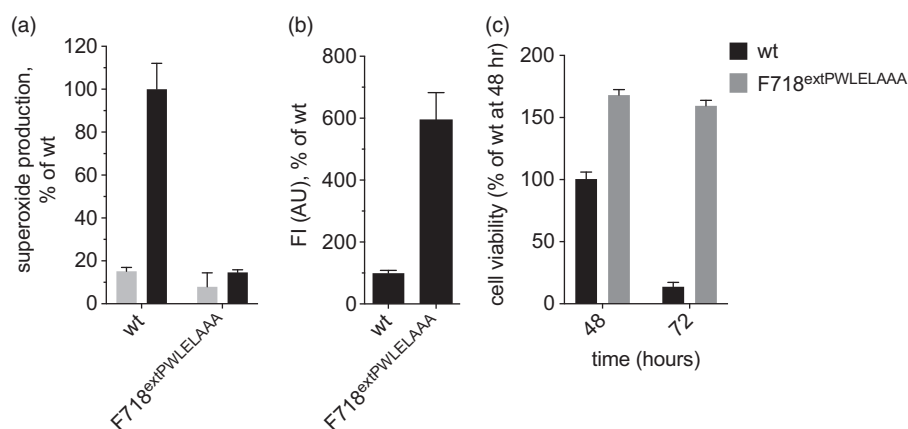
Figure 2 The insertion PWLELAAA increases human NOX5 production. 293HEK-F cells were transfected with either the human NOX5 wild type or NOX5-F718^{insPWLELAAA} cloned as a GFP fusion in a pCMV vector, as described in Methods. (A) Two days after transfection, superoxide production was measured in whole cells using the DHE assay: cells were either left untreated (gray) or NOX5 activation was induced by adding 1 mM CaCl2, 1 μM ionomycin, 100 nM PMA (black), as indicated in Methods. Fluorescence signal was recorded at the bottom of the plate using 524 nm excitation and 606 nm emission wavelengths for 40 min at 30 °C. The value corresponding to the 40-min time point was plotted. Values were normalized against the activated wild type (untreated: wt $=15 \pm 1\%$, F718$^{insPWLELAAA}=8 \pm 6\%$; Ca^{2+}-activated: wt $=100 \pm 12\%$, F718$^{insPWLELAAA}=14 \pm 1\%$). (B) The amount of enzyme produced in cells was obtained by measuring the fluorescence intensity of the GFP moiety genetically fused to the human NOX5 gene with 488 nm excitation and 520 nm emission wavelength. (C) Cell viability was evaluated by cell count using the Trypan Blue exclusion assay. The experiments were repeated three times in duplicates. Data are presented as mean values $\pm$ standard error of the mean (SEM).

served as control and was used for normalization. The height of the size-exclusion chromatography peak for each temperature was plotted to produce a melting curve (as described in Mancusso et al., 2011; Magnani et al., 2017). The apparent T_m is defined as the temperature where the peak height becomes half that of the control at 0 °C. The mutant csNOX5-F693^{extPWLELAAA} showed an increased app T_m of 8.3 ± 2.2 °C compared to the wild type (Figure 1(C); Table 2). Therefore, the C-terminal extension affects not only the autonomously folding dehydrogenase domain, but also the global stability of the full-length enzyme, whose transmembrane domain becomes more resilient to thermal denaturation, thus retaining more strongly the bound heme(s). In practical terms, an increase in T_m results in a more robust protein, which is expectedly better suited to withstand the purification process in detergent solution. In fact, the purified csNOX5 mutant was also less prone to aggregation (Figure 1(D)).

Transferability of the mutation to the human NOX5

Considering that the NOX family shares a high sequence conservation, particularly within the catalytic core, we grafted the PWLELAAA peptide after the Phe 718 C-terminal residue of the full-length human NOX5, which shares 40% identity with csNOX5 (Magnani

et al., 2017)\ and Figure 1B). The effect of the mutation was evaluated by overexpressing the wild-type and F718^{extPWLELAAA} NOX5s in HEK293 cells. As a first experiment, we probed the cells for superoxide production and protein expression (Figure 2). The levels of superoxide generation were clearly different between the two proteins, with the wild type exhibiting sevenfold higher ROS-producing activity compared to that measured on the cells expressing the F718^{extPWLELAAA} mutant (Figure 2(A)). On the other hand, the mutated protein displayed a noticeable increase in the expression levels, which were about six times higher than those obtained with cells expressing the wild-type enzyme (Figure 2(B)). Such enhanced expression of the mutant was partly correlated with increased cell viability (Figure 2(C)). Furthermore, the higher expression levels of F718^{extPWLELAAA} can also arise from a more efficient folding compared to the wild-type NOX5.

To further confirm the notion that engrafting the PWLELAAA C-terminal extension might be useful to improve stability, we subjected the human NOX5 enzymes to thermal stability assays. Since eukaryotic NOXs are harder to express and purify in milligram quantities than the bacterial csNOX5, we made use of the fluorescence of the GFP moiety fused at the enzymes N-terminus as a reporter for NOXs unfolding (Kawate & Gouaux, 2006). The detection of fluorescence with an in-line detector directly connected to
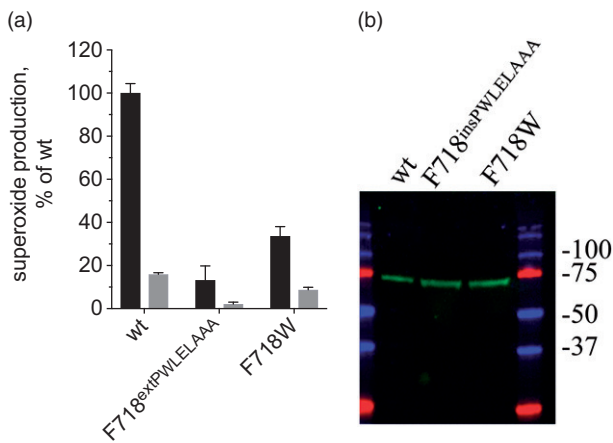
(a) (b)

Figure 3 The position of the inhibitory Trp is not fixed. HEK293-F cells were transfected as described in Methods with hNOX5 constructs cloned into the pEG-BacMam: wild-type hNox5 (wt) or mutants (F718^{insPWLELAAA} and F718W). (A) Superoxide measurement was carried out using the dihydroethidium assay as described in Figure 2(A). The value corresponding to the 40-min time point was plotted (values were normalized against the Ca^{2+}-activated wild-type human NOX5). Untreated cells (gray): wt $=15\pm1\%$, F718$^{insPWLELAAA}=2\pm1\%$, F718W$=9\pm1\%$; Ca^{2+}-activated cells (black): wt $=100\pm4\%$; F718$^{insPWLELAAA}=13\pm7\%$; F718W$=33\pm4\%$. Experiments were repeated three times in duplicates. Data are presented as mean values$\pm$SEM. (B) Western blotting analysis using an anti-FLAG antibody showed that the level of expression of the hNOX5 mutants is higher than the wild type.

the HPLC is much more sensitive than the absorbance at 414 nm of the heme prosthetic group. Also, since the GFP is genetically fused to the target gene, we can monitor the monodispersion of human NOXs on detergent-solubilized whole cells, avoiding purification (Kawate & Gouaux, 2006). The mutant showed a $2.6\pm1.1\,^{\circ}$C increase with respect to the T$_m$ of the wild type (Table 2). Though not as large as that observed for csNOX5, this effect is significant. Collectively, these data demonstrate that C-terminal extension strategy, initially discovered from the studies on the bacterial NOX5 homolog, can be fruitfully employed to obtain higher expression levels also for the human NOX5.

The beneficial effect of adding a C-terminal Trp residue is not strictly position dependent

The structural and biochemical analysis of the dehydrogenase domain from csNOX5 indicated that the Trp residue of C-terminally added PWLELAAA sequence is primarily responsible for increased thermal stability and reduced enzymatic activity exhibited by the mutant protein (Magnani et al., 2017) (Figure 1(A)). This residue is located in direct contact with the FAD to establish a stacking interaction between the indole

ring and the flavin (Figure 1(A)). Given these data, we were intrigued by the observation that the C-terminal amino acid of NOXs is often an aromatic residue (e.g. Phe718 in human NOX5 and Phe693 in csNOX5; Figure 1(B)). This feature becomes even more striking in light of the characteristic presence of a C-terminal aromatic residue among most members of the ferredoxin:NADP$^+$ reductase family to which the NOX's dehydrogenase domain belongs (Figure 1(B)) (Karplus et al., 1991; Zhen et al., 1998). By inspecting all available structures, it was noted that enzymes of the ferredoxin:NADP$^+$ reductase superfamily can often undergo local conformational changes that displace the C-terminal aromatic residue to allow NADPH binding during the catalytic cycle (Kean et al., 2017; Magnani et al., 2017).

We wondered whether in human NOX5 the substitution of the native Phe718 with a bulkier tryptophan would have the same effects observed for the F718^{extPWLELAAA} mutant, where the tryptophan is located within the longer PW^{720}LELAAA extension. We found that cells overexpressing F718W mutant protein display superoxide production levels that are twofold higher than those of the cells overexpressing F718^{extPWLELAAA} protein and threefold lower than those of the cells expressing wild-type human NOX5 (Figure 3(A)). Likewise, the F718W mutant exhibited similar expression levels compared to the classical F718^{extPWLELAAA} mutant, higher than those of the wild-type enzyme (Figure 3(B)). Therefore, the exact position of the tryptophan is not strictly important and a beneficial effect can be obtained also by mutating the C-terminal phenylalanine to a tryptophan. On the other hand, these effects are not as pronounced as those featured by the original F718^{extPWLELAAA} protein. Therefore, the PWLELAAA extension mutation was used for all subsequent studies on human NOX4.

The C-terminal mutation improves expression yields also on NOX4

Considering the high conservation of the catalytic domain across the NOX family (60% sequence identity among NOX1-5, 38% when also DUOX 1-2 are included (Magnani et al., 2017)), the original PWLELAAA was grafted over another member of the family, the human NOX4, an enzyme linked to several diseases, such as cancer (Fitzgerald et al., 2012), inflammation (Park et al., 2006), hypertension (Djordjevic et al., 2005), and atherosclerosis (Pedruzzi et al., 2004). Initially, ROS produced by NOX4 stimulate cell proliferation, but the progressive accumulation of
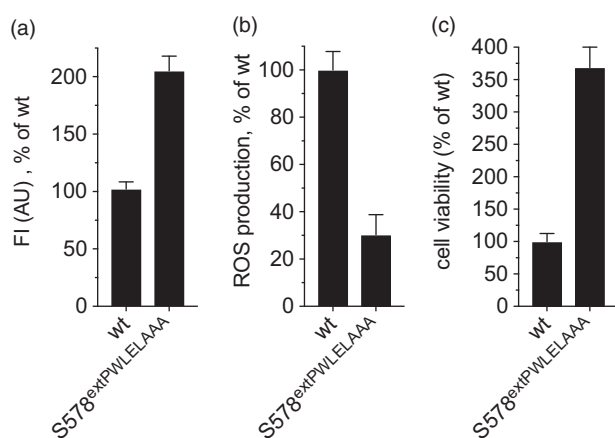
Figure 4 The insertion of the peptide PWLELAAA inhibits also human NOX4. Human NOX4 wild-type and mutant S578[insPWLELAAA] fused at the N-terminus to GFP were co-transfected with a plasmid carrying p22phox. (A) 48 h post-transfection, the expression of human NOX4 was evaluated by measuring GFP fluorescence with 488 nm excitation and 520 nm emission. (B) Activity measurements were performed by incubating the cells with Amplex Red and HRP; conversion to resorufin was measured after 40 min with 570 nm excitation and 585 nm emission. The value corresponding to the 40-min time point was plotted. (C) Cell viability was assessed 48 h post-transfection by counting the cells and the trypan blue exclusion. Experiments were repeated three times in duplicates. Data are presented as mean values ± SEM.

ROS elicits DNA damage response and replicative senescence (Ogrunc et al., 2014). Differently from NOX5 and DUOX1-2 but similar to NOX1-3, NOX4 does not have an N-terminal EF-calcium binding domain. NOX4 activity rather depends on the formation of a heterodimer with the accessory protein p22phox, and it is constitutively active in this heterodimeric form (Nisimoto et al., 2010; von Lohneysen et al., 2012). For this reason, cells were co-transfected with a plasmid encoding for p22phox. Moreover, the end product of NOX4 is proposed to be hydrogen peroxide (Nisimoto et al., 2014) and ROS-producing activities were therefore measured by means of the H_2O_2-sensing amplex red assay (Figure 4(B)).

Contrary to the other NOXs, the last natural amino acid of human NOX4 is not a phenylalanine but a serine (Ser578; Figure 1(B)). We decided to study the PWLELAAA extension in the context of the native enzyme, and thus, we placed the extension after Ser578. The yield of the mutated S578[extPWLELAAA] enzyme was about twofold higher than for the wild-type NOX4 (Figure 4(A)). As seen for the human NOX5, the C-terminally engrafted peptide had a significant effect on both ROS production and cell viability. Specifically, mutant NOX4-overexpressing cells had threefold lower ROS producing activity and more than

threefold higher viability compared to cells over-expressing wild-type NOX4 (Figure 4(B,C)). Conversely, S578[extPWLELAAA] did not induce any detectable protein-stabilizing effect (Table 2). We cannot discard the hypothesis that the characteristic Ser578 is important in sustaining the constitutive activity of human NOX4 and that it is the combination with an aromatic C-terminal residue that enables the stabilizing effect by the PWLELAAA C-terminal extension observed in NOX5 enzymes. Nevertheless, the data on protein expressing and ROS-producing activities indicate that the S578[extPWLELAAA] NOX4 variant can be useful for further biochemical and structural studies as its overexpression is less cell-toxic and yields high expression levels.

Discussion

The main hurdle to the biophysical and structural investigation of NOX's catalysis and regulation has been that overexpression of NOXs is toxic to cells (particularly for the expression in mammalian cells), with consequent loss of biomass and poor final protein yield. Moreover, membrane proteins can be challenging to work with due to their poor stability in detergent solution. This issue can become apparent during protein purification, or even during the solubilization of cell membranes, when the concentration of detergent is high and delipidation occurs. In fact, NOXs are prone to spontaneous proteolysis and tend to lose their non-covalently bound co-factors (FAD and hemes) during purification. Having observed the beneficial effect of the short peptide PWLELAAA added at the C-terminus of csNOX5 dehydrogenase domain (Magnani et al., 2017), we proceeded to further characterize this mutation in the broader context of the NOX family. The data shown here indicate that the stabilizing effect is not limited to the dehydrogenase domain but is transmitted to the transmembrane portion of the enzyme (Figure 1(C,D) and Table 2). The beneficial effect of the mutation F693[extPWLELAAA] in the full-length enzyme consists in a lower propensity to lose the heme group(s), a strict requirement to preserve the enzymatic capability of electron transport across the membrane to produce ROS.

Given this result and that within the NOX family the sequence identity of the catalytic core (transmembrane and dehydrogenase domains) is high, we further investigated the transferability of the PWLELAAA extension into the human NOX4 and NOX5. These two enzymes represent quite well the variation found within the NOX family with respect to the regulation of the catalytic activity. NOX4 is constitutively active,

whereas NOX5 (like DUOX1-2) is strongly regulated by its additional N-terminal calcium-binding EF hand domain, which allows its activation following an increase in the cytoplasmic Ca^{2+} concentration. NOX1-3 catalysis is also regulated, not by the EF hand domain but through cytosolic proteins. Similar to csNOX5, also human NOX5 is strongly stabilized by the PWLELAAA extension mutation (Table 2), with a very favorable six-fold increase in protein expression and improved cell viability associated to a reduced catalytic rate (Figure 2). The idea that this protein engineering strategy can become useful for further studies on NOXs found support in the experiments on human NOX4. The thermal stability of the protein was not changed by the PWLELAAA insertion but nonetheless the mutation significantly increased cell survival and protein expression by two-fold with a three-fold decrease in ROS-producing activity (Figure 4). To conclude, our work shows that a substantial improvement in the recombinant expression and stability of NOX enzymes is achieved; this should facilitate the development of selective drugs to modulate the function of NOXs, with the aim of discover novel therapeutic applications.

Acknowledgements

Disclosure statement

ORCID

Marta Ceccon http://orcid.org/0000-0002-4815-889X
Elisa Millana Fananas http://orcid.org/0000-0003-0513-8909
Marta Massari http://orcid.org/0000-0002-7731-7626
Andrea Mattevi http://orcid.org/0000-0002-9523-7128
Francesca Magnani http://orcid.org/0000-0003-0812-9397

References

Bedard K, Krause KH. 2007. The NOX family of ROS-generating NADPH oxidases: physiology and pathophysiology. Physiol Rev 87:245–313.

Block K, Gorin Y. 2012. Aiding and abetting roles of NOX oxidases in cellular transformation. Nat Rev Cancer 12:627–637.

Brown DI, Griendling KK. 2009. Nox proteins in signal transduction. Free Radic Biol Med 47:1239–1253.

de Mendez I, Leto TL. 1995. Functional reconstitution of the phagocyte NADPH oxidase by transfection of its multiple components in a heterologous system. Blood 85:1104–1110.

Djordjevic T, BelAiba RS, Bonello S, Pfeilschifter J, Hess J, Görlach A. 2005. Human urotensin II is a novel activator of NADPH oxidase in human pulmonary artery smooth muscle cells. Arterioscler Thromb Vasc Biol 25:519–525.

Doussiere J, Gaillard J, Vignais PV. 1999. The heme component of the neutrophil NADPH oxidase complex is a target for aryliodonium compounds. Biochemistry 38:3694–3703.

Fitzgerald JP, Nayak B, Shanmugasundaram K, Friedrichs W, Sudarshan S, Eid AA, et al. 2012. Nox4 mediates renal cell carcinoma cell invasion through hypoxia-induced interleukin 6- and 8- production. PLoS One 7:e30712.

Gao HM, Zhou H, Hong JS. 2012. NADPH oxidases: novel therapeutic targets for neurodegenerative diseases. Trends Pharmacol Sci 33:295–303.

Goehring A, Lee CH, Wang KH, Michel JC, Claxton DP, Baconguis I, et al. 2014. Screening and large-scale expression of membrane proteins in mammalian cells for structural studies. Nat Protoc 9:2574–2585.

Hattori M, Hibbs RE, Gouaux E. 2012. A fluorescence-detection size-exclusion chromatography-based thermostability assay for membrane protein precrystallization screening. Structure 20:1293–1299.

Irani K, Xia Y, Zweier JL, Sollott SJ, Der CJ, Fearon ER, et al. 1997. Mitogenic signaling mediated by oxidants in Ras-transformed fibroblasts. Science 275:1649–1652.

Isogai Y, Iizuka T, Shiro Y. 1995. The mechanism of electron donation to molecular oxygen by phagocytic cytochrome b558. J Biol Chem 270:7853–7857.

Karplus PA, Daniels MJ, Herriott JR. 1991. Atomic structure of ferredoxin-NADP + reductase: prototype for a structurally novel flavoenzyme family. Science 251:60–66.

Kawate T, Gouaux E. 2006. Fluorescence-detection size-exclusion chromatography for precrystallization screening of integral membrane proteins. Structure 14:673–681.

Kean KM, Carpenter RA, Pandini V, Zanetti G, Hall AR, Faber R, et al. 2017. High-resolution studies of hydride transfer in the ferredoxin:NADP(+) reductase superfamily. FEBS J 284:3302–3319.

Kuroda J, Ago T, Matsushima S, Zhai P, Schneider MD, Sadoshima J. 2010. NADPH oxidase 4 (Nox4) is a major source of oxidative stress in the failing heart. Proc Natl Acad Sci U S A 107:15565–15570.

Lambeth JD. 2004. NOX enzymes and the biology of reactive oxygen. Nat Rev Immunol 4:181–189.

Lambeth JD, Neish AS. 2014. Nox enzymes and new thinking on reactive oxygen: a double-edged sword revisited. Annu Rev Pathol 9:119–145.

Lord CI, Riesselman MH, Gripentrog JM, Burritt JB, Jesaitis AJ, Taylor RM. 2008. Single-step immunoaffinity purification and functional reconstitution of human phagocyte flavocytochrome b. J Immunol Methods 329:201–207.

Magnani F, Nenci S, Millana Fananas E, Ceccon M, Romero E, Fraaije MW, Mattevi A. 2017. Crystal structures and atomic

model of NADPH oxidase. Proc Natl Acad Sci U S A 114: 6764–6769.

Mancusso R, Karpowich NK, Czyzewski BK, Wang DN. 2011. Simple screening method for improving membrane protein thermostability. Methods 55:324–329.

Mittler R, Vanderauwera S, Suzuki N, Miller G, Tognetti VB, Vandepoele K, et al. 2011. ROS signaling: the new wave? Trends Plant Sci 16:300–309.

Nisimoto Y, Diebold BA, Cosentino-Gomes D, Lambeth JD. 2014. Nox4: a hydrogen peroxide-generating oxygen sensor. Biochemistry 53:5111–5120.

Nisimoto Y, Jackson HM, Ogawa H, Kawahara T, Lambeth JD. 2010. Constitutive NADPH-dependent electron transferase activity of the Nox4 dehydrogenase domain. Biochemistry 49:2433–2442.

O'Neill S, Brault J, Stasia M-J, Knaus UG. 2015. Genetic disorders coupled to ROS deficiency. Redox Biol 6:135–156.

Ogrunc M, Di Micco R, Liontos M, Bombardelli L, Mione M, Fumagalli M, et al. 2014. Oncogene-induced reactive oxygen species fuel hyperproliferation and DNA damage response activation. Cell Death Differ 21:998–1012.

Ohye H, Sugawara M. 2010. Dual oxidase, hydrogen peroxide and thyroid diseases. Exp Biol Med (Maywood) 235: 424–433.

Ostuni MA, Lamanuzzi LB, Bizouarn T, Dagher MC, Baciou L. 2010. Expression of functional mammal flavocytochrome b(558) in yeast: comparison with improved insect cell system. Biochim Biophys Acta 1798:1179–1188.

Park HS, Chun JN, Jung HY, Choi C, Bae YS. 2006. Role of NADPH oxidase 4 in lipopolysaccharide-induced proinflammatory responses by human aortic endothelial cells. Cardiovasc Res 72:447–455.

Pedruzzi E, Guichard C, Ollivier V, Driss F, Fay M, Prunet C, et al. 2004. NAD(P)H oxidase Nox-4 mediates 7-ketocholesterol-induced endoplasmic reticulum stress and apoptosis in human aortic smooth muscle cells. Mol Cell Biol 24:10703–10717.

Rotrosen D, Yeung CL, Katkin JP. 1993. Production of recombinant cytochrome b558 allows reconstitution of the phagocyte NADPH oxidase solely from recombinant proteins. J Biol Chem 268:14256–14260.

Rotrosen D, Yeung CL, Leto TL, Malech HL, Kwong CH. 1992. Cytochrome b558: the flavin-binding component of the phagocyte NADPH oxidase. Science 256:1459–1462.

Segal AW. 1987. Absence of both cytochrome b-245 subunits from neutrophils in X-linked chronic granulomatous disease. Nature 326:88–91.

Tom R, Bisson L, Durocher Y. 2008. Transfection of HEK293-EBNA1 cells in suspension with linear PEI for production of recombinant proteins. CSH Protoc 2008: pdb prot4977.

von Lohneysen K, Noack D, Hayes P, Friedman JS, Knaus UG. 2012. Constitutive NADPH oxidase 4 activity resides in the composition of the B-loop and the penultimate C terminus. J Biol Chem 287:8737–8745.

Weyemi U, Lagente-Chevallier O, Boufraqech M, Prenois F, Courtin F, Caillou B, et al. 2012. ROS-generating NADPH oxidase NOX4 is a critical mediator in oncogenic H-Ras-induced DNA damage and subsequent senescence. Oncogene 31:1117–1129.

Zhen L, Yu L, Dinauer MC. 1998. Probing the role of the carboxyl terminus of the gp91phox subunit of neutrophil flavocytochrome b558 using site-directed mutagenesis. J Biol Chem 273:6575–6581.

Zhu JK. 2016. Abiotic stress signaling and responses in plants. Cell 167:313–324.